Eur. Phys. J. C (2024) 84:1276
https://doi.org/10.1140/epjc/s10052-024-13649-x

THE EUROPEAN PHYSICAL JOURNAL C

Regular Article

Theoretical Physics

Geodesics of Finsler Hayward black hole surrounded by quintessence

B. R.Yashwanth[1,a], **S. K. Narasimhamurthy**[1,b], **Z. Nekouee**[2,c], **Manjunath Malligawad**[1,d]

[1] Department of PG Studies and Research in Mathematics, Kuvempu University, Shankaraghatta, Shivamogga, Karnataka 577 451, India
[2] School of Physics, Damghan University, Damghan 3671641167, Iran

Received: 12 April 2024 / Accepted: 24 November 2024

Abstract This research paper delves into examining the Hayward black hole structure surrounded by quintessence within the framework of Finsler geometry. Our focus centers on the Finsler metric tensor development for black holes. This newly derived metric introduces significant deviations from regular black hole metrics found in general relativity due to the Finslerian term γ presence, thus shedding fresh insights into the geometry and nature of black holes. Our findings reveal that the metric structure aligns closely with known Riemannian limits, affirming the congeniality of our model with existing theories. Furthermore, we extended our analysis to derive critical mass values and determine the normalization factor for the Hayward black hole within the Finlserian framework. The study encompasses a detailed description of the horizons and extremal conditions of the Hayward black hole surrounded by quintessence and the impact of the Finsler parameter γ on them. Specifically, we explore the case where the quintessence state parameter is set to $\omega = -2/3$. Our analysis delves into the effective potential, providing insights into null geodesics for various energy levels and examining the behavior of horizons by utilizing the definition of the effective potential. We also discuss the impact of γ for the same. We compute and analyze the radius of circular orbits, the period, the instability characteristics of circular orbits, and the force acting on photons with the newly introduced parameter γ within the quintessence field. We have thoroughly looked over the obtained results and discussed them. Additionally, we explore the shadow of the black hole in this context. Thereby, the validity and consistency of our Finslerian model are strengthened. In addition to increasing our understanding of black hole physics, this study paves the way for further research in the Finsler geometry domain and its applications in astrophysics.

1 Introduction

The exploration of black holes immersed in quintessence and the Finlserian parameter γ, a form of dark energy with unique properties, adds an intriguing dimension to our understanding of the cosmos. In this study, we delve into the characteristics of a black hole (BH) surrounded by quintessence and the impact of Finsler parameter γ, investigating its metric, horizons, and geodesics for different cases of γ. The incorporation of γ introduces novel features and complexities, influencing the structure and behavior of the BH. Quintessence, often described as a dynamic and evolving form of dark energy, plays a significant role in cosmic dynamics, affecting the universe's expansion. When coupled with a BH, both quintessence and γ can alter its horizons, gravitational potential, and even the trajectories of test particles, such as photons. Despite the event horizon concealing the singularities within the interior of BHs, it was predicted by Hawking years ago that the radiation flux from BHs leads to their gradual shrinkage until they eventually reach the singularity [1].

Researchers have proposed constructing a regular solution to address the singularity problem within BH solutions. One such approach involves combining the theory of general relativity with non-linear electrodynamics, where solutions devoid of a singularity at the center have been successfully formulated [2–4]. Another strategy for generating regular solutions is based on the notion that a regular solution should possess critical scale, mass, and charge parameters constrained by specific values. These values depend solely on the type of curvature invariant. This assumption is known as the limiting curvature conjecture [5].

[a] e-mail: yashmath0123@gmail.com
[b] e-mail: nmurthysk@gmail.com
[c] e-mail: zohrehnekouee@gmail.com (corresponding author)
[d] e-mail: manjunathmalligawad91@gmail.com

Published online: 09 December 2024

Building upon the concept of the limiting curvature, Hayward introduced a static spherically symmetric BH that exhibits behavior near the origin reminiscent of a de Sitter space-time [6]. The curvature invariants in this model remain finite throughout and adhere to the weak energy condition. Variations of this solution have been explored, such as the rotating Hayward [7] and Hayward-charged BHs [8]. Numerous investigations have also delved into the properties of the Hayward BH. For instance, in [9], the interior of the regular Hayward BH was examined using Painlev'e–Gullstrand coordinates, while [10,11] focused on studying the quasinormal modes associated with this BH.

Kiselev [12] introduced novel static spherically symmetric exact solutions to the Einstein equations, featuring quintessential matter surrounding a BH. This model has sparked various investigations, including [13], where the quasinormal models of a Schwarzschild BH enveloped by quintessence are explored. Additionally, [14] addresses null geodesics for a Schwarzschild BH surrounded by quintessence, while in [15] extends the study to Reissner–Nordstrom BHs surrounded by quintessence. In [16], a specific focus is placed on investigating the thermodynamics of a Hayward BH surrounded by quintessence. Recently, in [17], the geodesic incompleteness of Hayward's BH has been investigated. Besides this, researchers have also shown interest in examining the dynamics of the particles around a rotating BH and geodesic structures of regular BHs [18].

This research aims to unravel the intricacies of a BH immersed in quintessence, shedding light on how the interplay of gravitational forces and dark energy manifests in the vicinity of the event horizon. Through detailed analysis of metrics, horizon settings, and null geodesics, we seek to explain the distinctive properties and behaviors that arise when considering quintessence. By examining the effective potentials and the impact on null geodesics, we hope to contribute to the broader understanding of BHs in the presence of quintessence. In addition to deepening our understanding of fundamental astrophysical phenomena, such research paves the way for potential insights into the cosmic interaction between dark energy and BHs.

Finsler geometry, a generalization of Riemannian geometry with relaxed constraints on its metric [19–21], offers a broader range of geometrical objects and incorporates anisotropy, making it valuable for explaining small-scale anisotropies in the universe. Researchers have explored the universe through the lens of Finsler geometry, discussing gravity's nature within this framework. Modifications to the Friedmann–Robertson–Walker (FRW) metric reveal insights into the universe's inherent anisotropic characteristics. Extending the FRW model involves introducing anisotropic field structures dependent on position and direction, achieved through the osculating Riemannian approach to Randers spaces, portraying the universe within Finsler geometry. Thereby, research in Finsler geometry explores diverse aspects of the universe, offering unique perspectives distinct from Riemannian geometry and explaining a significant part of the observed universe through exact solutions derived from Einstein's field equations [22–24].

Presently, Finsler geometry holds considerable sway as a research domain. The intricate geometrical structures inherent in the Finsler geometry encompass a lot of complex objects, often necessitating significant time for computation. To mitigate these complexities, geometers have introduced the concept of osculation, particularly in exploring the universe using various models [26–28]. Hui-Ling Li et al. [25] delve into the remnant and its phase transition near the Planck scale within the framework of Finsler theory. Similarly, Chowdhury et al. scrutinize the characteristics of the non-commutative radiating Schwarzschild BH within Finslerian spacetime. Their investigation elucidates three possible scenarios for the BH: possessing two horizons, having a single horizon, or lacking a horizon, corresponding to a minimal mass state.

The outline of this paper unfolds in the following manner: The second section provides an introduction to the Finsler structure of the Hayward BH. In the third section, we discuss the critical mass and critical normalization factors, and an analysis of event horizons and extremal cases is provided. Moving to the fourth section, we explore the properties of the Hayward BH with quintessence, focusing on the case $\omega = -2/3$ and the Finsler parameter γ. In the fifth section, we delve into the study of null geodesics associated with these Finsler Hayward BH in the presence of quintessence, and we have also studied proper time, stability of circular geodesics, and force acting on photons, with examples showcasing different energy levels for various Finsler parameters. In the sixth section, we analyze the geodesics of Finsler Hayward BH for different values of γ. Subsequently, in the seventh section, a concise analysis of the shadow area of the Finsler Hayward BH surrounded by quintessence and the relation between the angular diameter Ω of the observed shadow and the constraint of the free parameter γ of a quintessence Finsler Hayward BH with $\omega = -\frac{2}{3}$ using the data from the Event Horizon Telescope (EHT) for Sagittarius A^* and $M87^*$ has been studied. Finally, the paper concludes with a summary of the findings in the last section.

2 Finsler structure of Hayward black hole

A Finsler metric, denoted by a real continuous function $\mathcal{F}(x, y)$, is defined on the tangent bundle TM of a smooth manifold M of n-dimensions with metric g_{ij} defined as

$$g_{ij} = \frac{\partial}{\partial y^i}\frac{\partial}{\partial y^j}\left(\frac{1}{2}\mathcal{F}^2\right). \tag{1}$$

The Finsler structure, defined by the function $\mathcal{F}(x, y)$, exhibits a property known as homogeneity, which is expressed by the equation: $\mathcal{F}(x, \mathrm{k}y) = \mathrm{k}\mathcal{F}(x, y)$ for $\mathrm{k} > 0$. The geodesic spray coefficients G^i, are expressed as follows

$$G^i = \frac{1}{4} g^{ik} \left(\frac{\partial^2 \mathcal{F}^2}{\partial x^\upsilon \partial y^k} y^\upsilon - \frac{\partial \mathcal{F}^2}{\partial x^k} \right). \tag{2}$$

The subsequent expression represents the geodesic equation within a Finsler manifold

$$\frac{d^2 x^i}{d\tau^2} + 2G^i = 0. \tag{3}$$

The expression for the Ricci scalar (Ric) [19] is given by

$$Ric \equiv R^j_j = \frac{1}{\mathcal{F}^2} \left(2\frac{\partial G^j}{\partial x^j} - y^i \frac{\partial^2 G^j}{\partial x^i \partial y^j} + 2G^i \frac{\partial^2 G^j}{\partial y^i \partial y^j} - \frac{\partial G^j}{\partial y^i} \frac{\partial G^i}{\partial y^j} \right). \tag{4}$$

The geometric invariant denoted by Ric mathematically can be represented as follows

$$Ric = g^{ij} R_{ij}. \tag{5}$$

Akbar-Zadeh [29] proposed a formulation for the modified Ricci tensor within the context of Finsler geometry. This tensor, denoted by Ric_{ij}, represents the curvature properties of a Finsler manifold and can be mathematically represented as

$$Ric_{ij} = \frac{\partial^2 \left(\frac{1}{2} \mathcal{F}^2 Ric \right)}{\partial y^i \partial y^j}. \tag{6}$$

Within this framework, the Finsler metric, represented as $\mathcal{F} = \mathcal{F}(x, y)$, is a function dependent on the coordinates (x^i, y^i) within a standard coordinate system. To incorporate angular coordinates, the following ansatz is employed, which encompasses $\bar{\mathcal{F}}^2 \left(\theta, \phi, y^\theta, y^\phi\right)$. Finsler metric is of the form

$$\mathcal{F}^2 = e^\lambda y^t y^t - e^\mu y^r y^r - r^2 \bar{\mathcal{F}}^2 \left(\theta, \phi, y^\theta, y^\phi\right). \tag{7}$$

Here, we consider functions $\lambda = \lambda(r)$ and $\mu = \mu(r)$ which depend only on radial coordinates. Additionally, it is noteworthy that $\bar{\mathcal{F}}$ remains invariant with respect to the coordinates y^t and y^r. Consequently, we can determine the coefficients of the Finsler metric using the following methodology.

$$g_{ik} = diag \left(e^\lambda, -e^\mu, -r^2 \bar{g}_{\mu\nu} \right), \tag{8}$$

$$g^{ik} = diag \left(e^{-\lambda}, -e^{-\mu}, -r^{-2} \bar{g}^{\mu\nu} \right). \tag{9}$$

The metric components $\bar{g}_{\mu\nu}$ and $\bar{g}^{\mu\nu}$, derived from $\bar{F}$, exhibit a dependence on the angular coordinates θ and ϕ. Utilizing the Finsler metric as defined in Eq. (7) and applying it to Eq. (2), we can deduce the geodesic spray coefficients, expressed as follows

$$G^t = \frac{1}{2} \lambda' y^t y^r,$$

$$G^r = \frac{\lambda'}{4} e^{\lambda-\mu} y^t y^t + \frac{\mu'}{4} y^r y^r - \frac{r}{2} e^{-\mu} \bar{\mathcal{F}}^2,$$

$$G^i = \frac{1}{r} y^i y^r + \bar{G}^i. \qquad (i = \theta, \phi) \tag{10}$$

In this context, $\bar{G}^i$ denotes the geodesic spray coefficient derived from $\bar{\mathcal{F}}$, and the prime notation indicates the derivative with respect to the radial coordinate r. Upon substituting the geodesic coefficients from Eq. (10) into Eq. (4), the resulting expression is as follows

$$\begin{aligned} Ric\mathcal{F}^2 = & \left[\frac{1}{2} \left(\lambda'' + (\lambda')^2 \right) e^{\lambda-\mu} - \frac{\lambda'}{4} e^{\lambda-\mu} (\lambda' + \mu') \right. \\ & \left. + \frac{\lambda'}{r} e^{\lambda-\mu}) \right] y^t y^t \\ & + \left[-\frac{1}{2} \left(\lambda'' + (\lambda')^2 \right) + \frac{\lambda'}{4} (\lambda' + \mu') + \frac{\mu'}{r} e^{-\mu} \right] y^r y^r \\ & + \left[Ric - e^{-\mu} + \frac{r}{2} e^{-\mu} (\mu' - \lambda') \right] \bar{\mathcal{F}}^2. \end{aligned} \tag{11}$$

The scalar curvature in Finsler geometry defined as

$$\begin{aligned} S = & g^{ik} Ric_{ik} \\ = & (\lambda'' + (\lambda')^2) e^{-\mu} - \frac{\lambda'}{2} e^{-\mu} (\mu' + \lambda') \\ & + \frac{2}{r} e^{-\mu} (\lambda' - \mu') - \frac{2}{r^2} \bar{Ric} + \frac{2}{r^2} e^{-\mu}. \end{aligned} \tag{12}$$

Pfeifer et al. [30] have investigated the gravitational dynamics within Finsler space-time using an action integral formulation on the unit tangent bundle. They observed that the gravitational field equation in Finsler space remains unaltered by the connection. This is attributed to the fact that the components $G_{\mu\nu}$ are obtained from the Ricci scalar, which fundamentally remains unaffected by the connections and is solely dependent on the Finsler structure. Consequently, the gravitational field equation in Finsler space can be expressed as follows:

$$G_{\mu\nu} = 8\pi_F G T_{\mu\nu}.$$

The fundamental tenets of General Relativity (GR), encompassing the gravitational interactions between matter and energy, are succinctly encapsulated by the Einstein field equations, which can be formulated as follows

$$G_{ik} = Ric_{ik} - \frac{1}{2} g_{ik} S = \kappa T_{ik}, \tag{13}$$

where $\kappa = 8\pi G_N$, G_N represents the Newton gravitational coupling constant. We represent the non-zero component of the energy-momentum tensor as

$$T^t_t = T^r_r = \rho, \tag{14}$$

$$T^\theta_\theta = T^\phi_\phi = -\frac{1}{2}(1 + 3\omega)\rho, \tag{15}$$

Here, ρ represents the system density, providing information about the distribution of mass or energy within it. On the

other hand, ω is the equation of state parameter, defining the connection between pressure and density. Furthermore, the dominating energy condition necessitates that $|3\omega + 1| \leq 2$ and $T_{tt} \geq 0$. Without sacrificing generality, we impose the condition $\mu = -\lambda$, where

$$\mu = -\ln(f(r)). \tag{16}$$

By implementing this condition and introducing the required adjustments to Eqs. (13) and (14), the following results are obtained [31]

$$G_t^t = G_r^r = -\frac{1}{r^2}\left(rf'(r) + f(r) - R\bar{i}c\right), \tag{17}$$

$$G_\theta^\theta = G_\phi^\phi = -\frac{1}{r^2}\left(\frac{1}{2}r^2 f''(r) + rf'(r)\right). \tag{18}$$

From the above hypothesis, the scalar curvature changes as

$$S = \frac{1}{r^2}\left(r^2 f''(r) + 4rf'(r) + 2f(r) - 2R\bar{i}c\right). \tag{19}$$

Incorporating the condition $R\bar{i}c = \gamma = constant$, the derivation for the Finslerian gravitational field equation leads as follows

$$\begin{aligned} &-\frac{1}{r^2}\left(rf'(r) + f(r) - \gamma\right) = \kappa\rho, \\ &-\frac{1}{r^2}\left(\frac{1}{2}r^2 f''(r) + rf'(r)\right) = -\frac{1}{2}(1+3\omega)\rho. \end{aligned} \tag{20}$$

Solving the set of differential equations (20) gives the solution for the Finslerian BH [31].

$$f(r) = \gamma - \frac{2M}{r} - \frac{\mathfrak{c}}{r^{1+3\omega}}, \tag{21}$$

along with we obtain the energy density of quintessence matter as follows

$$\rho = -\frac{3\mathfrak{c}\omega}{\kappa r^{3(1+\omega)}}. \tag{22}$$

Hayward proposed a model for the formation of BHs [6] that combines the concept of limiting curvature conditions with a minimal model. He formulated a regular, static, and spherically symmetric space-time to describe this formation process. Within this model, Hayward introduced a cosmological constant, denoted as Λ, into the Einstein tensor G_{ij}, particularly as $r \to 0$, represented as $G \sim -\Lambda g$. The value of Λ is determined to be $\frac{3}{\epsilon^2}$, where ϵ represents the Hubble length, effectively encoding the central energy density. Crucially, this cosmological constant ϵ introduces a significant effect, generating a repulsive force known as the repulsive core. This core plays a pivotal role in preventing the formation of a singularity at the center of the emerging BH.

By imposing specific conditions related to the Hayward BH [6] onto the spherically symmetric and static Finslerian metric expressed in Eq. (7), a solution is derived and presented in Eq. (21). This solution furnishes a mathematical description of the Finsler Hayward BH metric, denoted as $(\mathcal{F}_H)$.

$$\begin{aligned} \mathcal{F}_H^2 = {} & f_\omega(r) y^t y^t - \frac{1}{f_\omega(r)} y^r y^r - r^2 y^\theta y^\theta \\ & - r^2 \sin^2(\sqrt{\gamma}\theta) y^\phi y^\phi, \end{aligned} \tag{23}$$

where,

$$f_\omega(r) = \gamma - \frac{2Mr^2}{r^3 + 2M\epsilon^2} - \frac{\mathfrak{c}}{r^{3\omega+1}}. \tag{24}$$

The proved theorem in Ref. [32] shows that the two-dimensional Finsler space $\bar{\mathcal{F}}^2$ (see more details in Ref. [33]) has only one independent Killing vector, like the "Finslerian sphere" [32,34] that breaks isometric symmetry in Riemannian space-time. It is worth mentioning that this metric is a semi-definite Finsler space. As a result, we can use the covariant derivative of the Riemannian space. The Bianchi identities coincide with those of the Riemannian space (being the covariant conservation of Einstein tensor). One can find the gravitational field equations alternately [35]. Li et al. have also proved the covariance-preserving properties of the tensor G_ν^μ for the covariant derivative in Finsler space-time with the Chern-Rund connection.

The Ricci scalar depends only on the Finsler structure F and is insensitive to the connection. The gravitational field equation in the Finsler space is insensitive to the connection because the G_ν^μ are obtained from the Ricci scalar. Our paper studies the Hayward BH in Finsler geometry, which involves Riemannian geometry as a particular case. The Ricci scalar contributes to the geometry of the Finslerian Hayward BH structure. In our work, all the computations depend on. If $\gamma = 1$, the Finslerian Hayward BH structure reduces to the Riemannian case. Therefore, Finsler geometry promises a new way of analyzing the BH structure quite different from Riemannian, and we can see various works related to this metric in Refs. [36–39].

Within the $\mathcal{F}_H$ metric, $R\bar{i}c = \gamma = \text{constant}$, the term $\frac{\mathfrak{c}}{r^{3\omega+1}}$ signifies the quintessence term. Here, M denotes the mass of the Finslerian Hayward BH, ϵ is a parameter linked to the cosmological constant, ω represents the state parameter of the quintessence matter and $\mathfrak{c}$ serves as a positive normalization factor utilized in the metric equation. These symbols are employed to define and represent various parameters and characteristics associated with the Finslerian Hayward BH metric.

When $\mathfrak{c} = 0$ in the derived metric (23), the resulting metric is linked to the Finslerian Hayward BH. Conversely, when $\epsilon = 0$, this metric characterizes the Finslerian Schwarzschild (FSch) BH surrounded by quintessence matter [12,40]. Moreover, in the scenario where both $\mathfrak{c} = \epsilon = 0$, it exhibits behavior similar to the FSch BH [41], characterized by a single event horizon. It is essential to highlight that a variety of solutions for BHs can be derived by choosing dif-

ferent values for the parameter ω. For instance, $\omega = -1/3$ in the solution presented in Eq. (23) yields the Finslerian Hayward BH. Similarly, when $\omega = 1/3$ and $\mathfrak{c} = -Q^2$, this solution corresponds to the charged Finslerian Hayward BH. Specifically, the state parameter for quintessence lies within the range where $1 < \omega < -1/3$.

3 Event horizons of Finsler Hayward BH

The determination of horizons in the context of the Finsler Hayward BH with quintessence (Finsler Hayward BH-ω) involves finding the positive roots of the Eq. $f_\omega(r) = 0$. To facilitate analysis, we express key parameters such as the BH mass, radial distance, and the parameter $\mathfrak{c}$ in units of a constant ϵ. This involves the transformations $r \to r/\epsilon$, $M \to M/\epsilon$, and $\mathfrak{c} \to \mathfrak{c}/\epsilon^b$, where $b = 3\omega + 1$. The event horizons will be the roots of the equation

$$2Mr^{b+2} - \gamma r^{b+3} + \mathfrak{c}r^3 - 2M\gamma r^b + 2M\mathfrak{c} = 0. \tag{25}$$

The existence and number of horizons are contingent on the specific values chosen for the parameters ω, $\mathfrak{c}$, γ and M. Notably, the inclusion of the quintessence term introduces a novel horizon known as the cosmological (quintessence) horizon. Consequently, while the Hayward BH typically possesses two horizons, the Finsler Hayward BH-ω, with the addition of quintessence, may exhibit three horizons.

We adopt the methodology employed in [42,43] to ascertain the permissible range of values for the parameters M and $\mathfrak{c}$. This ensures that the line element describing the Finsler Hayward BH with quintessence (24) corresponds to a valid BH or an extremal BH.

Expressing the mass parameter as a function of r and $\mathfrak{c}$ based on Eq. (25), we aim to delineate the conditions under which the solution represents a BH or an extremal BH.

$$M(r,\mathfrak{c}) = \frac{1}{2}\frac{r^3\left(\gamma r^b - \mathfrak{c}\right)}{\left(r^{b+2} - \gamma r^b + \mathfrak{c}\right)}, \tag{26}$$

The mass parameter reaches an extremum at $\mathfrak{c}_{crit}$, as determined by

$$\mathfrak{c}_{crit} = \mathfrak{c}_\pm = \frac{1}{6}\left(\pm r^{1+b}\sqrt{(b-1)^2r^2 + 12b\gamma} + (b-1)r^{b+2} + 6\gamma r^b\right). \tag{27}$$

The variable $\mathfrak{c}_{crit}$ (27) exhibits extremal at specific r_{crit} values. Since $\mathfrak{c}_{crit} > 0$, the function $\mathfrak{c}_{crit}(r_{crit})$ must be positive within the range $-2 < b < 0$ because the condition is achieved when $-1 < \omega < -1/3$. By analyzing $\mathfrak{c}_{crit}(r_{crit})$, the extremum of $\mathfrak{c}_{crit} = \mathfrak{c}_+$ is identified at the $r_{crit} = \frac{\sqrt{6}}{2}\sqrt{\frac{\delta}{(b+2)(b-1)^2}}$, where $\delta = b^3\gamma - 6b^2\gamma - 11b\gamma + \sqrt{b^2\gamma^2(b^2-2b+17)(b+3)^2}$.

From now onwards we denote the critical value $\mathfrak{c}_{crit} = \mathfrak{c}_+$ of the quintessence parameter by $\mathfrak{c}_c$, r_{crit} by r_c and the critical mass $M_c = M(\mathfrak{c}_c, r_c)$ of the Finsler Hayward BH, in terms of ω and γ are given by;

$$M_c = -\frac{r_c^3\left(\sqrt{3}\sqrt{(3\omega^2r_c^2 + 12\gamma\omega + 4\gamma)r_c^{4+6\omega}} + 3\omega r_c^{3\omega+3}\right)}{(6\omega+12)r_c^{3\omega+3} + 2\sqrt{3}\sqrt{(3\omega^2r_c^2 + 12\gamma\omega + 4\gamma)r_c^{4+6\omega}}}, \tag{28}$$

$$\mathfrak{c}_c = \frac{1}{6}\left(\sqrt{3}\sqrt{(3\omega^2r^2 + 12\gamma\omega + 4\gamma)r^{4+6\omega}} + 3\omega r^{3\omega+3} + 6\gamma r^{3\omega+1}\right), \tag{29}$$

$$r_c = \frac{\sqrt{2}}{6}\sqrt{\frac{(27\omega^3 - 27\omega^2 - 60\omega - 16)\gamma + \sqrt{(3\omega+1)^2\gamma^2(9\omega^2+16)(4+3\omega)^2}}{(\omega+1)\omega^2}}. \tag{30}$$

The behavior of the critical values $\mathfrak{c}_c$ and M_c with respect to ω for different values of γ, as depicted in Fig. 1, reveals that with an increase in ω, $\mathfrak{c}_c$ also increases, while M_c decreases for all the values of γ as shown in the Fig. 1.

For values of $\mathfrak{c} \leq \mathfrak{c}_c$, the Finlser Hayward BH with ω exhibits diverse horizon configurations. It is noteworthy that as $\omega \to -1$, $\mathfrak{c}_c \to \frac{1}{24}$ for all $\gamma > 0$ (Fig. 1a). Consequently, for small ω values, both $\mathfrak{c}_c$ and M_c remain finite. On the other hand, as $\omega \to -\frac{1}{3}$, $M_c \to 0$ for all $\gamma > 0$ (Fig. 1b). This limit implies that, in the presence of quintessence, the likelihood of BH formation diminishes.

The extremal of the Finsler Hayward BH-ω solution can be determined by satisfying the condition $f_\omega(r) = 0$, where,

$$\frac{d}{dr}f_\omega(r) = \frac{4b\left(\frac{r^3}{2} + M\right)^2\mathfrak{c}r^{-1-b} + 2Mr^4 - 8M^2r}{(r^3+2M)^2} = 0. \tag{31}$$

By substituting the expression for $M(r,\mathfrak{c})$ from Eq. (26) into Eq. (31), we derived the resulting condition.

$$\gamma(r^2 - 3\gamma)r^{2b} + \mathfrak{c}((b-1)r^2 + 6\gamma)r^b - 3\mathfrak{c}^2)r^7 = 0. \tag{32}$$

If certain values of ω, γ and $\mathfrak{c}_c$ are chosen, Eq. (32) can yield two real roots denoted as r_+ and r_-. In such cases, then

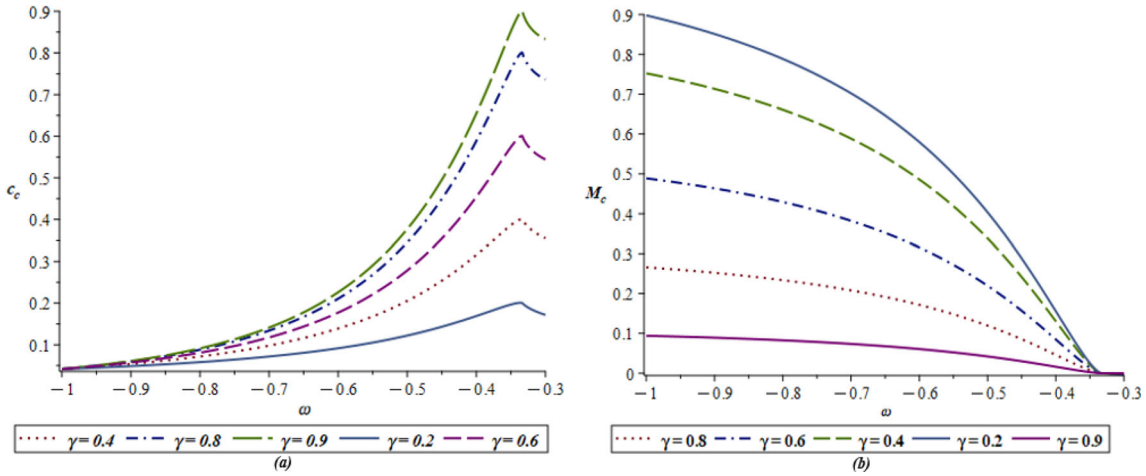

Fig. 1 Behaviour of $\mathfrak{c}_c$ and M_c for different values of γ with $-1 < \omega < -1/3$

the mass (26) takes the following form:

$$M(r_+, \mathfrak{c}) = \frac{1}{2}\frac{r_c^3(\gamma r_+^b - \mathfrak{c})}{(r_+^{b+2} - \gamma r_+^b + \mathfrak{c})}, \tag{33}$$

$$M(r_-, \mathfrak{c}) = \frac{1}{2}\frac{r_c^3(\gamma r_-^b - \mathfrak{c})}{(r_-^{b+2} - \gamma r_-^b + \mathfrak{c})}, \tag{34}$$

The subsequent section provides an analysis illustrating the behavior of Eqs. (33) and (34) for various γ values, specifically with $\omega = -2/3$. The conditions corresponding to certain ω and γ values are summarized in Table 1, depicting the values of $\mathfrak{c}_c$ and M_c. This Table clearly illustrates how both ω and γ factors influences the horizons of the Finsler Hayward BH-ω. It is evident that on keeping γ fixed at lower values say $\gamma = 0.2$, an increase in the ω value leads to a decrease in the critical values of normalization factor $\mathfrak{c}_c$, accompanied by an increase in the corresponding critical mass values (M_c) of Finsler Hayward BH. Similarly, for higher values of γ with γ fixed at 0.8, an increase in ω results in a decrease in the critical values of normalization factor $\mathfrak{c}_c$ and a simultaneous increase in the corresponding critical mass values (M_c) of Finsler Hayward BH. Therefore, it can be concluded that for any positive γ, an increase in the ω (from $-4/9$ to $-8/9$) values leads to a decrease in $\mathfrak{c}_c$ values and an increase in the corresponding (M_c) as shown in the Fig. 1. For a more detailed analysis of the Finsler Hayward BH-ω behavior with quintessence, it is essential to select a specific ω value. In this context, we propose choosing $\omega = -2/3$, as it yields an intermediate value of M_c.

Table 1 The values of $\mathfrak{c}_{crit}$ and M_{crit} are computed for various ω and γ values

ω	γ	$\mathfrak{c}_{crit}$	M_{crit}
$-4/9$	0.2	0.14585	0.02874
	0.4	0.25987	0.02874
	0.6	0.36434	o.14934
	0.8	0.46305	0.22993
$-1/2$	0.2	0.12212	0.04225
	0.4	0.20538	0.11951
	0.6	0.27837	0.21956
	0.8	0.34540	0.33804
$-5/9$	0.2	0.10357	0.05336
	0.4	0.16441	0.15093
	0.6	0.21544	0.27728
	0.8	0.26099	0.42690
$-2/3$	0.2	0.07753	0.06977
	0.4	0.10964	0.19736
	0.6	0.13429	0.36258
	0.8	0.15506	0.55823
$-7/9$	0.2	0.06081	0.08084
	0.4	0.07662	0.22866
	0.6	0.08771	0.42008
	0.8	0.09653	0.64675
$-8/9$	0.2	0.04956	0.08853
	0.4	0.05562	0.25042
	0.6	0.05951	0.46006
	0.8	0.06244	0.70831

4 Finsler Hyward black holes with $\omega = -2/3$

Our attention is now directed towards the specific case of $\omega = -2/3$, allowing for a relatively straightforward examination of the characteristics of Finsler Hayward BH with quintessence and along with the parameter γ.

The horizons are determined for $\omega = -2/3$ by solving Eq. (35) (i.e., setting $f_\omega(r) = 0$).

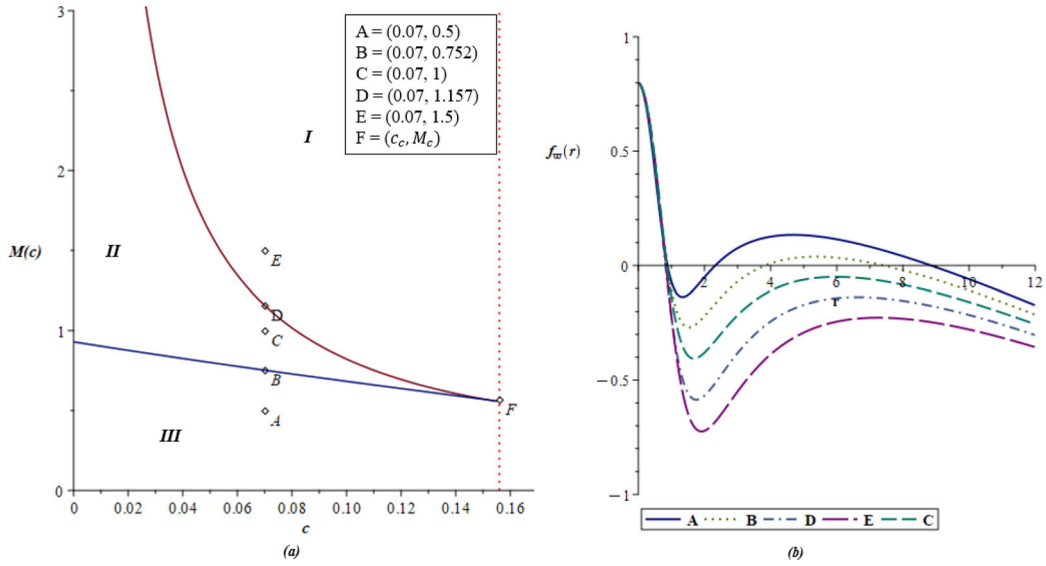

Fig. 2 **a** The behavior of M as function of $\mathfrak{c}$ is shown for $\omega = -2/3$ and $\gamma = 0.8$. **b** The function metric $f_\omega(r)$ for the values of M and $\mathfrak{c}$

$$2Mr^2 - \gamma r^3 + \mathfrak{c}r^4 - 2M\gamma + 2M\mathfrak{c}r = 0. \tag{35}$$

For a certain value of $\mathfrak{c} = \mathfrak{c}_c = 0.15506$, there exist three real positive roots, namely r_{in}, r_{out}, and r_q. Now, Eq. (32) for $\omega = -2/3$ can be expressed as:

$$2\mathfrak{c}r^3 + (3\mathfrak{c}^2 - \gamma)r^2 - 6\mathfrak{c}\gamma r = -3\gamma^2. \tag{36}$$

Eq. (36) is a cubic equation and may exhibit two real positive roots, and is given by,

$$r_+ = \frac{1}{6\mathfrak{c}}\sum + \frac{1}{6\mathfrak{c}}\frac{(9c^4 + 30\gamma\mathfrak{c}^2 + \gamma^2)}{\sum} - \frac{1}{6\mathfrak{c}}(3\mathfrak{c}^2 - \gamma), \tag{37}$$

$$r_- = -\frac{1}{12\mathfrak{c}}\sum - \frac{1}{12\mathfrak{c}}\frac{(9\mathfrak{c}^4 + 30\gamma\mathfrak{c}^2 + \gamma^2)}{\sum} - \frac{1}{6\mathfrak{c}}(3\mathfrak{c}^2 - \gamma) - \frac{I\sqrt{3}}{12\mathfrak{c}}\sum + \frac{1}{12\mathfrak{c}}\frac{(9\mathfrak{c}^4 + 30\gamma\mathfrak{c}^2 + \gamma^2)}{\sum}I\sqrt{3}, \tag{38}$$

where, $\sum = (-27\mathfrak{c}^6 - 135\mathfrak{c}^4\gamma - 117\gamma^2\mathfrak{c}^2 + 18\gamma\sqrt{\gamma(9\mathfrak{c}^4 + 33\gamma\mathfrak{c}^2 + \gamma^2)}\mathfrak{c} + \gamma^3)^{\frac{1}{3}}$. Generally, the various roots follow the relation $r_{in} \le r_- \le r_{out} \le r_+ \le r_q$, where r_q represents the quintessence horizon.

Figure 2a illustrates the behavior of M as a function of $\mathfrak{c}$ for $\omega = -2/3$. In regions I and II, the Finsler Hayward BH-ω features a single horizon, while in region III, there are three horizons. The boundary between regions I and II corresponds to the extremal Finsler Hayward BH-ω ($M(r_+)$), and the boundary between regions II and III corresponds to the extremal Finsler Hayward BH-ω ($M(r_-)$). Additionally, in Fig. 2b, the metric function $f_\omega(r)$ is depicted for various values of M and $\mathfrak{c}$ within regions I, II, and III, considering $M(r_+)$ and $M(r_-)$.

Depending on the values of the parameters M, $\mathfrak{c}$ and γ, the number of horizons may decrease from three to one. The cosmological (quintessence) horizon r_q never vanishes, and when only this singular horizon remains, the Finsler Hayward BH-ω describes a naked singularity. It is worth noting that the introduction of the quintessence term, $-\mathfrak{c}/r^{3\omega+1}$, leads to a decrease in the critical mass, i.e., $M_c < M_*$ as in Table 1. To further enhance the understanding of the horizons of Finsler Hayward BH-ω, we supplement the analysis by examining the behavior of $M(r, \mathfrak{c})$ Eq. (26) with $\omega = -2/3$.

$$M_\omega(r) = M(r, \mathfrak{c}) = \frac{1}{2}\frac{r^3(\gamma - \mathfrak{c}r)}{(\mathfrak{c}r + r^2 - \gamma)}. \tag{39}$$

It's important to note that the function $M_\omega(r) \to 0$ as $r \to 0$. As $r \to \infty$, $M_\omega(r) \to -\infty$, and there is a discontinuity in $M_\omega(r)$ at $r_h = [\sqrt{\mathfrak{c}^2 + 4\gamma} - \mathfrak{c}]/2$. The behavior of the function $M_\omega(r)$ for a specific value of $\mathfrak{c}$ is illustrated in Fig. 3.

As depicted in Fig. 3, two critical values, $M_{\omega min}$ and $M_{\omega max}$, emerge for the mass of the Finsler Hayward BH-ω, leading to distinct physical scenarios. Firstly, for $M_\omega < M_{\omega min}$, a naked singularity is observed. When $M_\omega = M_{\omega min}$ (or $M_{\omega max}$), a Finsler Hayward BH-ω with two horizons is present. For M_ω values between $M_{\omega min}$ and $M_{\omega max}$, three horizons are observed. For a specific M_ω value, such as 1.5, the Finsler Hayward BH-ω features three horizons: the inner horizon r_{in}, the event horizon r_{out} (where $r_{out} \ge r_{in}$), and the quintessence horizon r_q (where $r_q \ge r_{out}$). When the normalization factor $\mathfrak{c}_c$ is at its critical value of 0.15506, the Finsler Hayward BH-ω exhibits a single horizon, i.e., $r_{in} = r_{out} = r_q$. These BHs are referred to as ultra-cold BHs [44,45]. For values of $\mathfrak{c} > \mathfrak{c}_c$, no BH exists for any M_ω value. Conversely, for the values $\mathfrak{c} < \mathfrak{c}_c$, BHs may have two or three horizons, but only for M_ω values falling within the

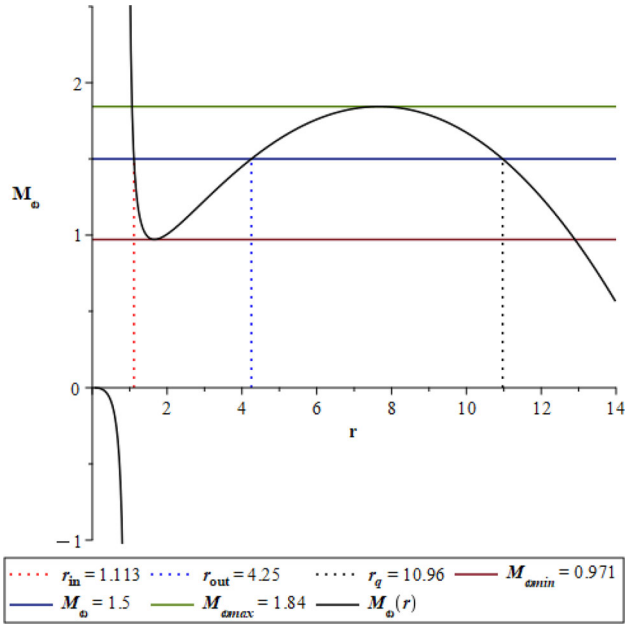

Fig. 3 The figure shows the horizons of the Finsler Hayward BH-ω with $\mathfrak{c}$=0.045 and $\gamma = 0.8$

range of $M_{\omega min}$ to $M_{\omega max}$. Here, $M_{\omega min}$ and $M_{\omega max}$ represent the minimum and maximum local values, respectively, of the expression $M_\omega(r)$. When $M_\omega = M_{\omega max}$, the situation corresponds to the Nariai BH, as discussed in Ref. [46].

$$r_{out} = r_q = -\frac{(3\mathfrak{c}^2-\gamma)}{6\mathfrak{c}} + \frac{(\gamma^2+30\gamma\mathfrak{c}^2+9\mathfrak{c}^4)}{6\mathfrak{c}\Delta} + \frac{\Delta}{6\mathfrak{c}}, \tag{40}$$

where, $\Delta = (\gamma^3 - 27\mathfrak{c}^6 - 135\mathfrak{c}^4\gamma - 117\gamma^2\mathfrak{c}^2 + 18\gamma\sqrt{\gamma(9\mathfrak{c}^4+33\gamma\mathfrak{c}^2+\gamma^2)}\mathfrak{c})^{\frac{1}{3}}$.

When $M_\omega = M_{\omega min}$, we get,

$$r_{in} = r_{out} = -\frac{(3\mathfrak{c}^2-\gamma)}{6\mathfrak{c}} - \frac{\Delta}{12\mathfrak{c}} - \frac{(\gamma^2+30\gamma\mathfrak{c}^2+9\mathfrak{c}^4)}{12\mathfrak{c}\Delta} - I\frac{\sqrt{3}}{12\mathfrak{c}} + I\frac{(\gamma^2+30\gamma\mathfrak{c}^2+9\mathfrak{c}^4)}{12\mathfrak{c}\Delta}. \tag{41}$$

5 Null geodesics equation with $\omega = -2/3$

In this section, we will obtain the null geodesics for the Finsler Hayward BH-ω. Considering spherical coordinates $x^\mu = (t, r, \theta, \phi)$. From Eq. (3), it can be proven that the Finslerian structure $\mathcal{F}(x, \frac{dx}{d\tau})$ along the geodesic is constant [26,27]. The geodesic equations are expressed with this condition as follows,

$$g_{\mu\nu}u^\mu u^\nu = \mathcal{F}^2$$

where $\dot{x}^\mu \equiv \frac{dx^\mu}{d\tau} = u^\mu$. It is possible to consider $2\mathcal{L} = \mathcal{F}^2$, and if $\mathcal{F} = 1$, it corresponds to time-like geodesics, while $\mathcal{F} = 0$ corresponds to null geodesics. So, the motion of test particles along geodesics is described by the Lagrangian density $\mathcal{L} = \frac{1}{2}\dot{x}^\mu\dot{x}_\mu$, where "dot" indicates the first derivative with respect to the affine parameter τ. Utilizing the form of the line element (23) and the expression of $f_\omega(r)$ given by Eq. (24), the Lagrangian density can be expressed as:

$$\mathcal{L} = \frac{1}{2}\left(f_\omega(r)\dot{t}^2 - \frac{\dot{r}^2}{f_\omega(r)} - r^2\dot{\theta}^2 - r^2\sin^2(\sqrt{\gamma}\theta)\dot{\phi}^2\right), \tag{42}$$

The equation of motion is given by,

$$\dot{\Pi}_{x^\mu} - \frac{\partial\mathcal{L}}{\partial x^\mu} = 0. \tag{43}$$

Here, $\Pi_{x^\mu} = \frac{\partial\mathcal{L}}{\partial\dot{x}_\mu}$ represents the momentum corresponding to the coordinate x^μ. As the Lagrangian is independent of t and ϕ, two conserved quantities will arise:

$$\Pi_t = -f_\omega(r)\dot{t} = -E, \tag{44}$$

$$\Pi_\phi = r^2\sin^2(\sqrt{\gamma}\theta)\dot{\phi} = L, \tag{45}$$

where E and L represent constants of motion corresponding to energy and angular momentum, respectively.

We examine the motion on the plane with $\theta = \pi/2$, and by utilizing Eqs. (44) and (45), the Lagrangian given in Eq. (42) can be expressed as:

$$2\mathcal{L} \equiv \mathcal{F}^2 = \frac{E^2}{f_\omega(r)} - \frac{\dot{r}^2}{f_\omega(r)} - \frac{L^2}{r^2\sin^2(\sqrt{\gamma}\frac{\pi}{2})}. \tag{46}$$

By solving the above equation for $\dot{r}^2$, we get,

$$\dot{r}^2 = E^2 - f_\omega(r)\left(h + \frac{L^2}{r^2\sin^2(\sqrt{\gamma}\frac{\pi}{2})}\right). \tag{47}$$

In this study, our focus will be solely on null geodesics ($h = 0$). Hence, the equation describing null geodesics for the Finsler Hayward BH-ω is provided by:

$$\dot{r}^2 = E^2 - V_{eff}, \tag{48}$$

or

$$\frac{dr}{d\phi} = \frac{r^2\sin^2(\sqrt{\gamma}\frac{\pi}{2})}{L}\sqrt{E^2 - V_{eff}}. \tag{49}$$

Here, $V_{eff} = f_\omega(r)\frac{L^2}{r^2\sin^2(\sqrt{\gamma}\frac{\pi}{2})}$. The effective potential V_{eff} for the Finsler Hayward BH-ω with $\omega = -2/3$ can be expanded as:

$$V_{eff} = \frac{L^2}{r^2\sin^2(\sqrt{\gamma}\frac{\pi}{2})}\left(\gamma - \frac{2Mr^2}{r^3+2M\epsilon^2} - \mathfrak{c}r\right). \tag{50}$$

It is evident that $V_{eff} \to 0$ as $r \to \infty$. Figure 4 illustrates the effective potential of null geodesics for various values of γ. Notably, the shape of the potential remains consistent, regardless of the specific values of γ. It can be noted that

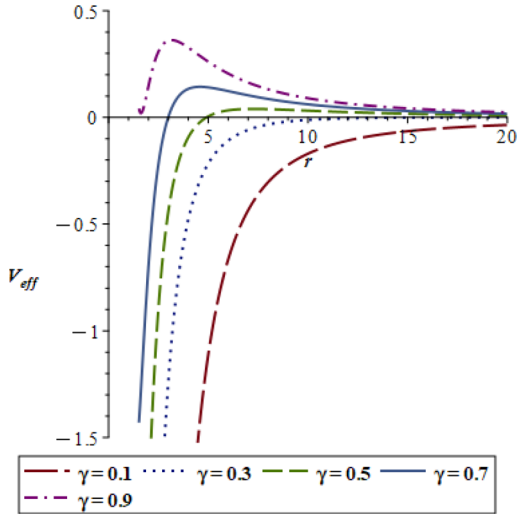

Fig. 4 The figure shows V_{eff} for different values of γ with $L = 20$, $M = 1$ and $\epsilon = 1$

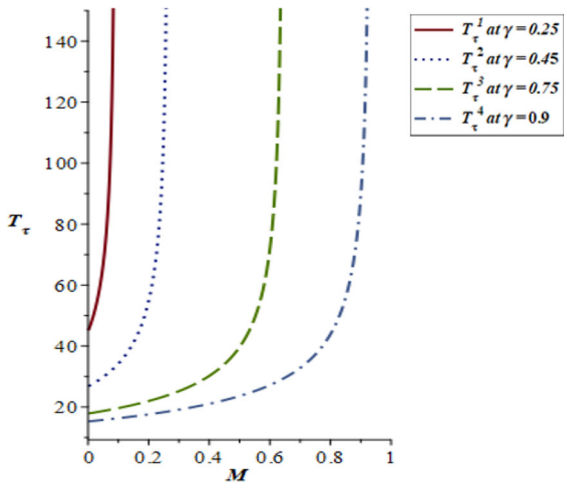

Fig. 5 T_τ as a function of M for Finsler Hayward BH-ω surrounded by quintessence for different values of γ with $\mathfrak{c} = 0.1$ and $\omega = -2/3$

as the parameter γ increases for the Finsler Hayward BH-ω, the influence of the gravitational potential diminishes. In Fig. 4, the potential exhibits maxima, indicating the presence of unstable null geodesics with a radius of r_c. Thus, three distinct scenarios can be considered based on the values of E for the motion:

- In the first scenario, $E^2 - V_{eff} = 0$ implies $\dot{r} = 0$, leading to the existence of circular null geodesics. To determine whether these null geodesics are stable or unstable, certain conditions must be satisfied: $V'_{eff}(r_C) = V_{eff}(r_C) = 0$, where r_C is the radius of the circular orbit. Here, the symbol '$\prime$' indicates the derivative with respect to r. Additionally, for circular stable orbits, the condition $V''_{eff}(r_C) > 0$ must be achieved, and $V''_{eff}(r_C) < 0$ for unstable orbits. Generally, the conditions for obtaining stable or unstable geodesics are:

$$\frac{E}{L} = \pm\left[\frac{1}{2r_C \sin^2(\sqrt{\gamma}\frac{\pi}{2})}\left(\frac{2Mr_C(r_C^3 - 4M\epsilon^2)}{(r_C^3 + 2M\epsilon^2)^2} - \mathfrak{c}\right)\right]^{1/2}. \tag{51}$$

  For instance, it is conceivable to choose $E = E_C$, which corresponds to the maximum value of V_{eff} located at r_C.
- In the second case, $E_1^2 - V_{eff} > 0$ for all r. This situation corresponds to the energy value $E = E_1$ associated with open null geodesics.
- In the third case, $E_2^2 - V_{eff} < 0$ for all r. This scenario corresponds to the energy value $E = E_2$ associated with closed null geodesics.

It is worth noting that the effective potential $V_{eff} \to 0$ as $r \to r_{in}, r_{out}$, and r_q. When two horizons coincide, the maximum of the effective potential becomes zero. In this study, we will specifically focus on examining the behavior of photons in the presence of non-degenerate horizons.

5.1 Proper time period

The period of circular orbits encompasses the time required for a particle to complete one full revolution around the circular path. The formulas for calculating the period of proper time T_τ are derived from the equation provided by Fernando in 2012 [14].

$$T_\tau = \frac{2\pi r_C}{\sqrt{f_\omega(r)}}. \tag{52}$$

The period for Finsler Hayward BH-ω surrounded by quintessence for different values of γ is plotted in Fig. 5.

From the Fig. 5 it is found that proper time for Finsler Hayward BH-ω is highest at $\gamma = 0.29$ when compared to the other greater values of γ, while it attain lowest at $\gamma = 0.95$. We can see that,

$$T_\tau^4 < T_\tau^3 < T_\tau^2 < T_\tau^1.$$

5.2 Stability of circular geodesics

The Lyapunov exponent λ serves as a metric for assessing the stability or instability of circular geodesics. In cases where λ is a real value, it indicates the instability of the circular orbit. The time scale for the instability of circular null geodesics is quantified by the Lyapunov exponent λ, and its computation is determined by the equation provided by Cardoso et al. [47].

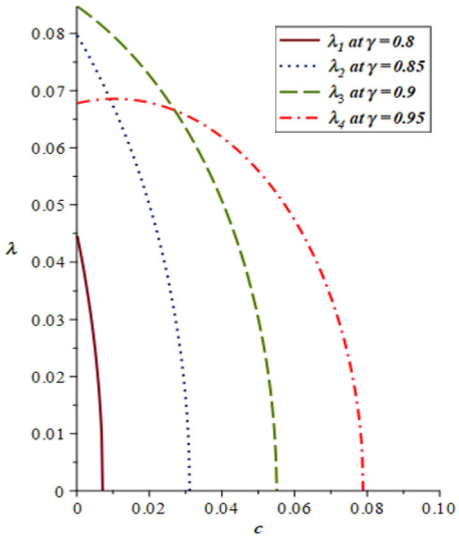

Fig. 6 Lyapunov exponent λ as a function of $\mathfrak{c}$ for Finsler Hayward BH-ω surrounded by quintessence for different values of γ with $M = 1.2$, $L = 4$ and $\omega = -2/3$

$$\lambda = \sqrt{\frac{-V''_{eff}(r_C) r^2 f_\omega(r)}{2L^2}}. \tag{53}$$

Lyapunov exponent λ of Finsler Hayward BH-ω surrounded by quintessence for different values of γ is plotted in Fig. 6. According to Fig. 6, it can be found that the instability of the circular orbits of the Finsler Hayward BH at $\gamma = 0.9$ is the greatest compared to the other lower values of γ for the greater values of $\mathfrak{c}$, while the instability of the circular orbits of Finsler Hayward BH at $\gamma = 0.8$ is the lowest compared to the other values of γ for the greater values of $\mathfrak{c}$. From the Fig. 6 it is clear that,

$$\lambda_4 > \lambda_3 > \lambda_2 > \lambda_1.$$

5.3 Force acting on photons

Determining the force acting on photons can be achieved by utilizing the definition of the effective potential, as outlined by Fernando [14].

$$F_\alpha = -\frac{1}{2}\frac{dV_{eff}}{dr}. \tag{54}$$

From Fig. 7, we can see that the force factor is more positive at $\gamma = 0.9$ and it is more negative at $\gamma = 0.3$, i.e.,

$$F^4_\alpha > F^2_\alpha > F^3_\alpha > F^1_\alpha.$$

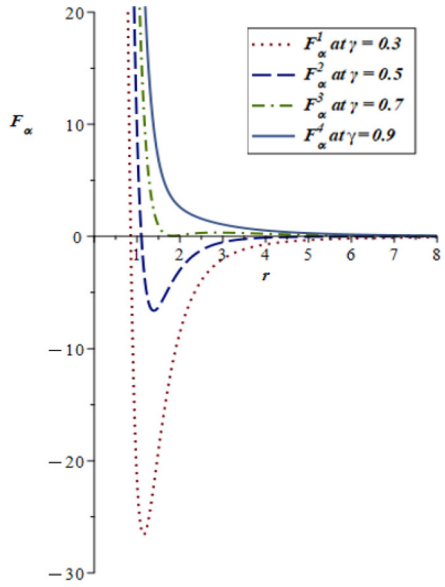

Fig. 7 F_α behavior as a function of r for Finsler Hayward BH-ω surrounded by quintessence for different values of γ with $M = 0.5$, $L = 10$, $\mathfrak{c} = 0.1$ and $\omega = -2/3$

6 Analyzing the geodesics of Finsler Hayward BH

To analyze the geodesic equation of motion (49), we aim to simplify the study of orbits by introducing a change of variable. Letting $u = \frac{1}{r}$, we can then express Eq. (49) as:

$$\left(\frac{du}{d\phi}\right)^2 = g(u), \tag{55}$$

where $g(u)$ corresponds to

$$g(u) = \frac{E^2 \sin^4(\sqrt{\gamma}\frac{\pi}{2})}{L^2} - u^2\gamma \sin^2(\sqrt{\gamma}\frac{\pi}{2}) + \frac{2Mu^3 \sin^2(\sqrt{\gamma}\frac{\pi}{2})}{1 + 2M\epsilon^2 u^3} + \mathfrak{c}u \sin^2(\sqrt{\gamma}\frac{\pi}{2}), \tag{56}$$

or

$$g(u) = \frac{\sin^2(\sqrt{\gamma}\frac{\pi}{2})}{L^2\left(1 + 2M\epsilon^2 u^3\right)}\Big[- 2M\epsilon^2 u^5 \gamma L^2 + 2L^2\mathfrak{c}\epsilon^2 u^4 + 2M\left(E^2\epsilon^2 \sin^2(\sqrt{\gamma}\frac{\pi}{2}) + L^2\right)u^3 - L^2u^2\gamma + L^2\mathfrak{c}u + E^2 \sin^2(\sqrt{\gamma}\frac{\pi}{2})\Big], \tag{57}$$

$g(u)$ can be written as:

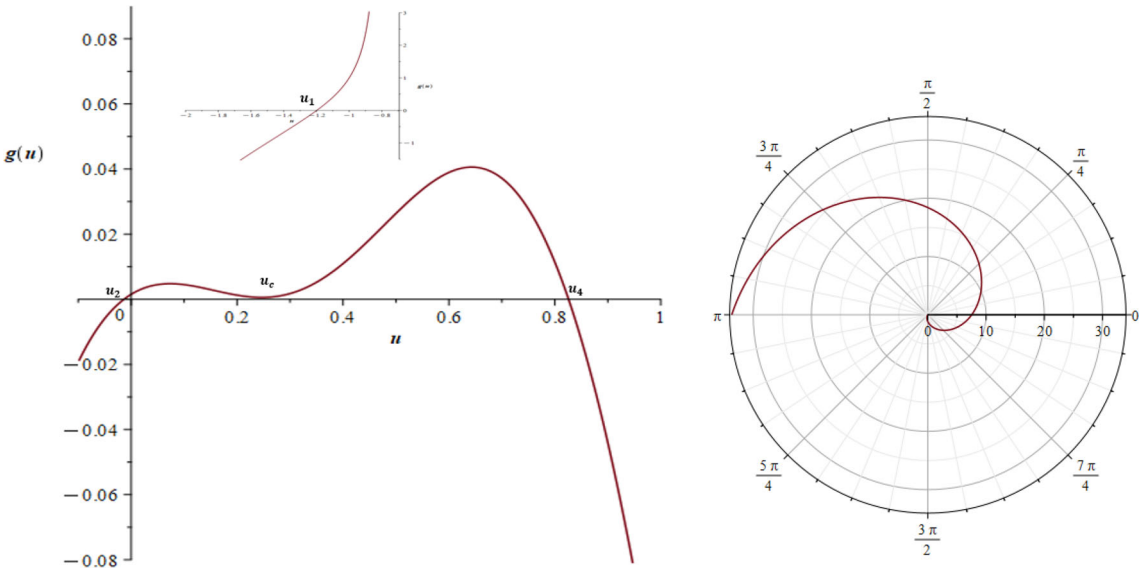

Fig. 8 The geodesic have an unstable circular orbit at $r = r_C$. Here $E_C = 1.00125$, $L = 25.6$, $M = 1$, $\epsilon = 1$, $\gamma = 0.9$ and $\mathfrak{c} = 0.1$

$$g(u) = \frac{-2L^2M\epsilon^2\gamma \sin^2(\sqrt{\gamma}\frac{\pi}{2})(u-u_1)(u-u_2)(u-u_3)(u-u_4)(u-u_5)}{L^2\left(1+2ML^2\epsilon^2u^3\right)\gamma}, \tag{58}$$

here, u_i represents the roots of $g(u)$, and $u_1u_2u_3u_4u_5 = \frac{E^2\sin^2(\sqrt{\gamma}\frac{\pi}{2})}{2ML^2\epsilon^2}$. The geometry of the null geodesics is contingent upon the roots of the function $g(u)$. It's important to note that, for any values of the parameters M, ϵ, $\mathfrak{c}$, E, γ and L, the function $g(u) \to \pm\infty$ as $u \to \infty$. Additionally, when $u \to 0$, $g(u) \to \frac{E^2\sin^2(\sqrt{\gamma}\frac{\pi}{2})}{L^2}$. Consequently, $g(u)$ has three positive roots and two negative roots. The geometry of the geodesics is intricately linked to the roots of the function $g(u)$. By numerically solving Eq. (55) with appropriate boundary conditions, one can discern the paths followed by massless particles in the Finlser Hayward BH-ω.

- When a test particle, such as a photon, approaches from $r_D > r_C$, it experiences an unstable circular orbit at $r = r_C$. The associated motion is depicted in Fig. 8. Notably, when considering the values of $E = E_C$, the function $g(u)$ exhibits a degenerate root $u_C = \frac{1}{r_C}$, as illustrated in Fig. 8, where the graph for $g(u)$ displays four roots.
- When considering $E = E_1$, the photons, for all values of r, exhibit a trajectory leading them into the BH, as depicted in Fig. 9. In this scenario, the function $g(u)$ features two imaginary and three real roots, as illustrated in the graph of $g(u)$ in Fig. 9.
- If $E = E_2$, the test particle initiates its journey far from the Finsler Hayward BH-ω at $u_D = \frac{1}{r_D}$. It then falls until $u_{out} = \frac{1}{r_{out}}$ and subsequently moves away from the BH. Figure 10 illustrates this situation, where $g(u)$ has five real roots.

7 The shadow of Finsler Hayward BH-ω with $\omega = -2/3$

The shadow of a BH in the observer's sky appears dark when the light sources are situated anywhere in the universe except between the observer and the BH. The shape of the shadow can provide crucial information about the parameters of the BH. As depicted in Fig. 4, the behavior of the effective potentials reveals the existence of photon spheres. Given the spherically symmetric nature of the Finsler Hayward BH-ω, the shadow is circularly symmetric and depends solely on the impact parameter, defined as $b_C^2 = \frac{L^2}{E^2}$ [48]. The impact parameter b_C is related to the effective potential by $V_{eff}(r_C) = \frac{1}{b_C^2}$. The connection between the shadow area and the impact parameter is expressed as $\sigma = \pi b_C^2$.

By combining Eq. (51) with the definition of the shadow area, the impact parameter is given by:

$$\frac{1}{b_C^2} = \pm\frac{1}{2r_C\sin^2(\sqrt{\gamma}\frac{\pi}{2})}\left(-\mathfrak{c} + \frac{2Mr_C(r_C^3-4M\epsilon^2)}{(r_C^3+2M\epsilon^2)^2}\right) \tag{59}$$

Figure 11 illustrates the variation in the shadow area of the Finsler Hayward BH-ω, comparing it with different values of γ. It is significant that the introduction of the scalar factor γ and the quintessence state parameter ω leads to an increase in the shadow area. As we can see in Fig. 11, as the values of

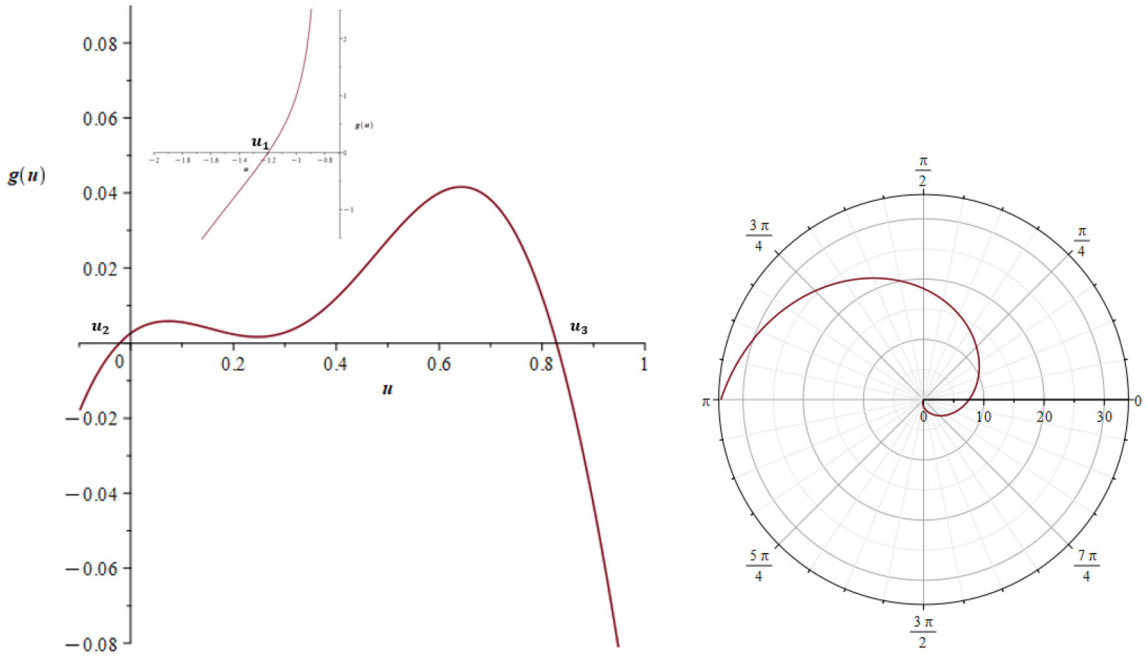

Fig. 9 The geodesic have an unstable circular orbit at $r = r_C$. Here $E_C = 1.30125$, $L = 25.6$, $M = 1$, $\epsilon = 1$, $\gamma = 0.9$ and $\mathfrak{c} = 0.1$

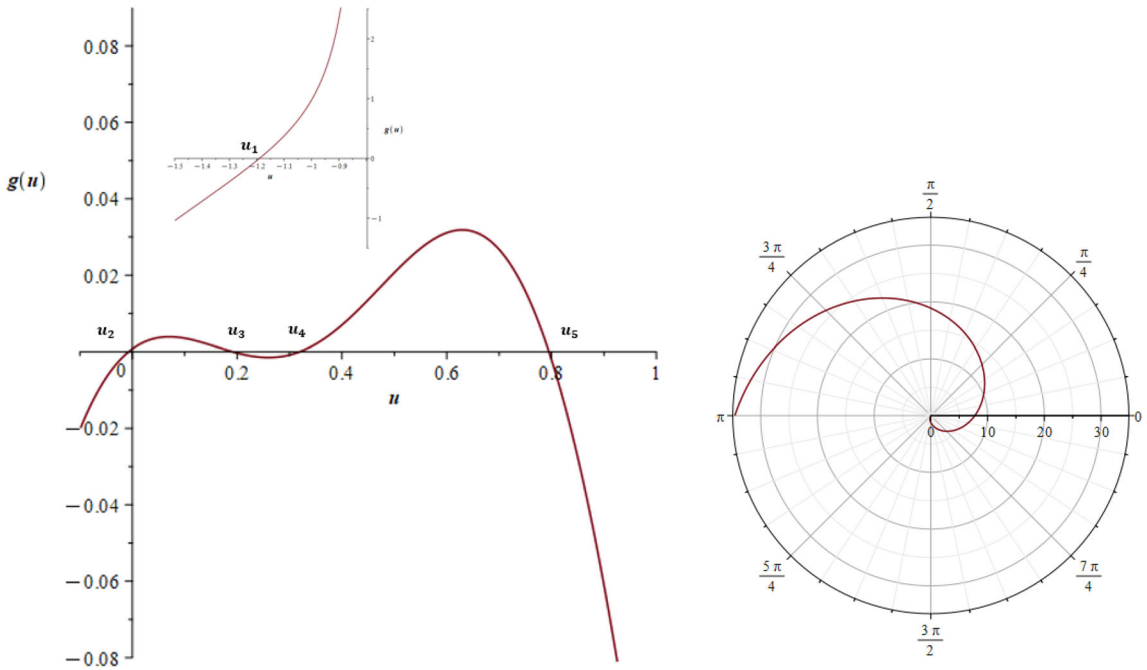

Fig. 10 The geodesic have an unstable circular orbit at $r = r_C$. Here $E_C = 0.70125$, $L = 25.6$, $M = 1$, $\epsilon = 1$, $\gamma = 0.9$ and $\mathfrak{c} = 0.1$

γ increase, the Finsler Hayward BH-ω shadow area becomes greater.

This suggests that the shadow area expands as the factor γ increases. However, it is essential to note that the range of r_c decreases for lower values of γ, signifying a broader range of parameter combinations E, L, M, and ϵ to achieve photospheres with a radius of r_c. In 2016, Abdujabbarov et al. [49] investigated the shadow of a rotating Hayward BH, and Lopez et al. [10] discussed the shadow of a charged Hayward BH.

To determine the photon sphere and the impact parameter for the quintessence Finsler Hayward BHs using the ray-tracing method, we will consider the photon orbit occurring at $r = r_C$. Consequently, the conditions for these orbits,

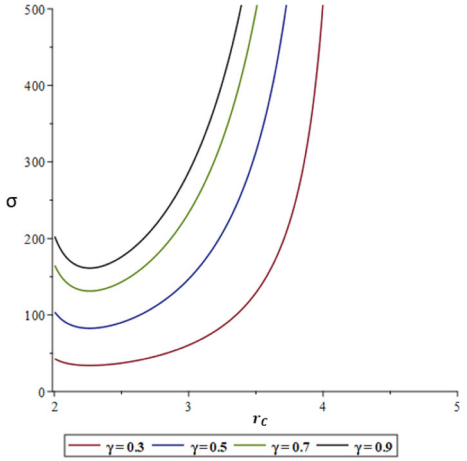

Fig. 11 The shadow area of Hayward BH-ω with $M = 1$, $\mathfrak{c} = 1$ and $\epsilon = 1$, for different values of γ

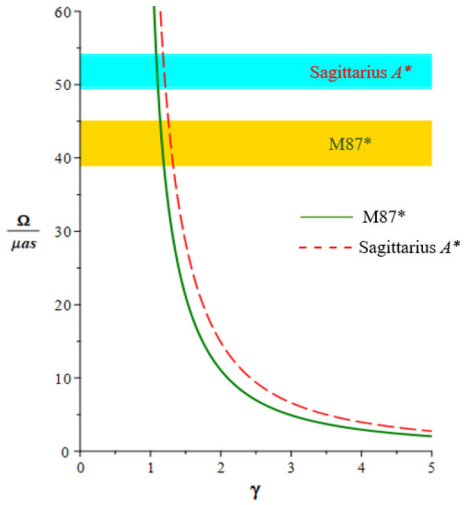

Fig. 12 The relation between the angular diameter Ω of the observed shadow and the parameter γ of a quintessence Finsler Hayward BH with $\omega = -\frac{2}{3}$

derived from Eq. (47), are given by

$$V_{eff}(r_C) = E_C^2, \quad V'_{eff}(r_C) = 0. \tag{60}$$

Use of Eq. (50) leads to the following relation

$$r f'_\omega(r) - 2 f_\omega(r) = 0. \tag{61}$$

Substituting $f_\omega(r)$ from Eq. (24) we obtain the following equation for the photon sphere

$$\gamma r^6 - 3Mr^5 + 4M\epsilon^2\gamma r^3 + 4\gamma M^2\epsilon^4 - \frac{3}{2}\mathfrak{c}(\omega+1)\left(2M\epsilon^2 + r^3\right)^2 r^{-(3\omega+1)} = 0. \tag{62}$$

The above equation lacks an analytical solution, so we numerically determine its roots. For $\mathfrak{c} = \epsilon = 0$, we find $r_C = 3M$, corresponding to the photon radius in Schwarzschild spacetime. When $\mathfrak{c} = 0$ and $\epsilon \neq 0$, specifically for Finsler Hayward BHs, which also lacks an analytical solution. However, for Schwarzschild BHs in the presence of quintessence matter with $\mathfrak{c} \neq 0$ and $\epsilon = 0$, there is an exact solution for $\omega = -\frac{2}{3}$, given by:

$$r_C = \frac{1 - \sqrt{1 - 6M\mathfrak{c}}}{\mathfrak{c}}. \tag{63}$$

Moreover, the impact parameter of the photon sphere, defined as $b_C = L_C/E_C$, was given by [50]

$$b_C = \frac{r_C}{\sqrt{f_\omega(r_C)}}. \tag{64}$$

Since the shadow is a distinct characteristic of the space-time metric, it can be used to constrain the parameters of the space-time geometry based on the observed shadow [51–56]. The angular diameter Ω of the BH shadow, as seen by a distant observer, can be defined as follows [51]

$$\Omega = \frac{2b_C}{D}, \tag{65}$$

where D is the distance between the BH and the distant observer. The above equation can be rewritten as

$$\left(\frac{\Omega}{\mu as}\right) = \left(\frac{6.191165 \times 10^{-}8}{\pi}\frac{\chi}{D/Mpc}\right)\left(\frac{b_C}{M}\right), \tag{66}$$

here χ is the ratio of the BH to the Sun, and the impact parameter of the photon sphere, b_C, is obtained from the Eq. (64).

For quintessence Finsler Hayward BHs, one can obtain constraints of the free parameters using the shadow diameter estimated by the EHT observations. We consider the quintessence Finsler Hayward BH ($\epsilon = 0.9$) with $\omega = -\frac{2}{3}$ and constrain the parameter γ for both $M87^*$ and Sagittarius A^* in the Fig. 12. Current observations correspond to $\chi = 4.14 \times 10^9$ and a distance $D = 8.127$ kpc for Sagittarius A^*, and $\chi = 6.2 \times 10^9$ and a distance $D = 16.8$ Mpc for $M87^*$, respectively [57,58]. The yellow and blue regions represent the shadow diameters of $M87^*$ ($42 \pm 3\mu as$) and Sagittarius A^* ($51.8 \pm 2.3\mu as$) as reported by the EHT observations. Consequently, we constrain the parameter γ of the quintessence Hayward BH is constrained to $1.13866 < \gamma < 1.1909$ for $M87^*$, and $1.17908 < \gamma < 1.21421$ for Sagittarius A^*.

Figure 12 represents the relation between the angular diameter Ω of the observed shadow and the constraint of the free parameter γ of a quintessence Finsler Hayward BH with $\omega = -\frac{2}{3}$. The green (solid) curve corresponds to the theoretical shadow diameter predictions for $M87^*$, and the red (dashed) curve corresponds to the theoretical shadow diameter predictions for Sagittarius A^*. In essence, the plot visually demonstrates how the theoretical prediction of the BH shadow diameters, influenced by the parameter γ, align with the empirical observations from the EHT, thereby constrain-

ing the values of γ to specific ranges for both $M87^*$ and Sagittarius A^*.

8 Results and conclusions

In this study, we investigate the metric of the Finsler Hayward BH surrounded by quintessence matter. To analyze the horizons of the new solution, we provide critical values for the $\mathfrak{c}$ (normalization factor) and M (mass) parameters in terms of ω and γ. Additionally, considering the introduction of the quintessence term and γ, we identify the emergence of a new horizon, and the conditions for a Finsler Hayward BH-ω extremal are also examined. The dependence of the mass on the value of $\mathfrak{c}$ for different values of γ is presented in the analysis.

We investigate the null geodesics of BHs surrounded by quintessence and analyze the influence of γ on the null geodesics of Hayward BHs. By examining the structure of these geodesics, we extract several physical properties of this BH. Initially, we provide a concise introduction and present the structure of Finsler Hayward BH under consideration. The horizons are determined using the methodology outlined by Kiselev. Specifically, we apply this approach to quantify the horizons for the parameter value of $\omega = -2/3$. This new horizon is linked intricately to the parameter ω. We delve into the analysis of regions where the Finsler Hayward BH with quintessence possesses one, two, or three horizons for some $\gamma > 0$, specifically in the case of $\omega = -2/3$. Importantly, it is observed that the cosmological (quintessence) r_q horizon persists without vanishing. In this particular instance, the Finsler Hayward BH with quintessence describes a naked singularity. Additionally, it is noteworthy that the critical mass decreases with $M_c < M_*$.

Using the concept of the effective potential, we computed various parameters such as the radius of circular orbits, the period, the instability of circular orbits, and the force exerted on photons in the presence of quintessence under the influence of γ. Our analysis and discussions revealed several key findings. Firstly, we observed that the effective potential for higher values of γ of the Finsler Hayward BH surrounded by quintessence exhibited the highest value among the considered other lower values of γ. Secondly, we found that the radius of circular orbits and the period for lower values γ of the Finsler Hayward BH surrounded by quintessence is the largest compared to other higher values of γ. Furthermore, it can be found that the instability of the circular orbits of the Finsler Hayward BH for higher values γ is the greatest compared to the other lower values of γ for the greater values of $\mathfrak{c}$. Moreover, we determined that the force exerted on photons for the higher values γ is the greatest compared to other lower values of γ of the Finsler Hayward BH surrounded by quintessence.

To analyze the geodesic equation of motion, we employed the variable change $u = \frac{1}{r}$. The trajectories of photons can be confined within the quintessence horizon. But if they extend beyond the horizon $r = r_{out}$, the photons plunge into the BH, thus designating the quintessence horizon as an apparent horizon. In conclusion, it is noted that the shadow area increases with an increase in the factor γ. We also constrained the amount of the free parameter of the quintessence Finsler Hayward BH with $\omega = -\frac{2}{3}$ compatible with the EHT observations of Sagittarius A^* and $M87^*$ supermassive BHs.

Acknowledgements The author Yashwanth B. R. acknowledges OBC Fellowship, Backward Classes Welfare Department (BCWD), Govt. of Karnataka, India, for the financial support in the form of OBC-Ph.D Fellowship (Application No:2021PHD1755402).

Author contributions Yashwanth B. R.: Analysis, Plotting graphs, Writing manuscript. S. K. Narasimhamurthy: Editing and Analysis. Z. Nekouee: Editing, Analysis, and Plotting some graphs. Manjunath Malligawad: Reviewing and Editing. Yashwanth B. R.: https://orcid.org/0000-0002-8239-5741 S. K. Narasimhamurthy: https://orcid.org/0000-0002-2711-4636 Z. Nekouee: https://orcid.org/0000-0003-3126-2321 Manjunath Malligawad: https://orcid.org/0000-0002-6306-8489

Funding There is no funding for this work.

Data availability Statement The authors confirm that the data supporting the findings of this study are available within the article.

Code Availability Statement The manuscript has no associated code/software. [Author's comment: Code/Software sharing not applicable to this article as no Code/Software was generated or analysed during the current study.]

Declarations

Conflict of interest No potential Conflict of interest was reported by authors.

Ethics approval and consent to participate All authors approve ethics, and all authors consent to participate.

Consent for publication All authors consent for publication.

References

1. S.B. Giddings, S.D. Thomas, Phys. Rev. D **65**, 056010 (2002)
2. J.M. Bardeen, Non-singular general-relativistic gravitational collapse, in *Proceedings of International Conference GR5*, Tbilisi, USSR (1968), p. 174
3. K.A. Bronnikov, Phys. Rev. D **63**, 044005 (2001)
4. I. Dymnikova, Class. Quantum Gravity **21**, 4417 (2004)
5. J. Polchinski, Nucl. Phys. B **325**, 619 (1989)
6. S.A. Hayward, Phys. Rev. Lett. **96**, 031103 (2006)
7. M. Amir, S.G. Ghosh, JHEP **07**, 015 (2015)
8. V.P. Frolov, Phys. Rev. D **94**, 104056 (2016)
9. I. Perez-Roman, N. Breton, Gen. Relativ. Gravit. **50**, 64 (2018)
10. L.A. Lopez, V. Hinojosa, Can. J. Phys. **99**, 44 (2021)
11. K. Lin, J. Li, S. Yang, Int. J. Theor. Phys. **52**, 3771 (2013)
12. V.V. Kiselev, Class. Quantum Gravity **20**, 1187 (2003)
13. S. Chen, J. Jing, Class. Quantum Gravity **22**, 4651 (2005)
14. S. Fernando, Gen. Relativ. Gravit. **44**, 1857 (2012)
15. B. Malakolkalami, K. Ghaderi, Mod. Phys. Lett. A **30**, 1550049 (2015)
16. K.K.J. Rodrigue, M. Saleh, B.B. Thomas, T.C. Kofane, Mod. Phys. Lett. A **35**, 2050129 (2020)
17. T. Zhou, L. Modesto, Phys. Rev. D **107**, 044016 (2023)
18. J. Hu, Y. Zhang, L. Shi, P. Duan, Gen. Relativ. Gravit. **50**, 89 (2018)
19. D. Bao, S.S. Chern, Z. Shen, *An Introduction to Riemann–Finsler Geometry* (Springer, New York, 2000)
20. S.S. Chern, Z. Shen, *Riemann–Finsler Geometry*, vol. 6 (World Scientific Publishing Company, Singapore, 2005)
21. S.S. Chern, Finsler geometry is just Riemannian geometry without the quadratic restriction (1997)
22. P.C. Stavrinos, J. Phys. Conf. Ser. **8**(01), 49 (2005)
23. P.C. Stavrinos, A.P. Kouretsis, M. Stathakopoulos, Gen. Relativ. Gravit. **40**, 1403 (2008)
24. P.C. Stavrinos, A.P. Kouretsis, J. Phys. Conf. Ser. **68**(01), 012023 (2007)
25. H.-L. Li, Z.-W. Feng, S.-Z. Yang, X.-T. Zu, Eur. Phys. J. C **78**, 768 (2018)
26. H.M. Manjunatha, S.K. Narasimhamurthy, S.K. Srivastava, Pramana **97**, 90 (2023)
27. X. Li, Z. Chang, Phys. Rev. D **90**, 064049 (2014)
28. S.K. Narasimhamurthy, Z. Nekouee, H.M. Manjunatha, Indian J. Phys. **97**, 279 (2023)
29. H. Akbar-Zadeh, Acad. R. Belg. Bull. Cl. Sci. **74**, 281 (1988)
30. C. Pfeifer, M.N.R. Wohlfarth, Phys. Rev. D **85**, 064009 (2012)
31. Z. Nekouee, S.K. Narasimhamurthy, Eur. Phys. J. C **83**, 723 (2023)
32. H.C. Wang, J. Lond. Math. Soc. **s1-22**, 5 (1947)
33. F. Rahaman, N. Paulb, A. Banerjeec, S.S. De, S. Raye, A.A. Usmani, Eur. Phys. J. C **76**, 246 (2016)
34. X. Li, Phys. Rev. D **98**, 084030 (2018)
35. X. Li, S. Wang, Z. Chang, Commun. Theor. Phys. **61**, 781 (2014)
36. N. Ksh, F. Singh, D. Rahaman, S.K. Deb, [Maurya], Front. Phys. **10**, 1038905 (2023)
37. H.M. Manjunatha, S.K. Narasimhamurthy, Chin. J. Phys. **77**, 1561 (2022)
38. M. Malligawad, S.K. Narasimhamurthy, Z. Nekouee, M.Y. Kumbar, Phys. Scr. **99**, 045206 (2024)
39. T. Sanjay, S.K. Narasimhamurthy, Z. Nekouee, H.M. Manjunatha, [Pramana], J. Phys. **98**, 16 (2024)
40. X. Li, X. Zhang, H.-N. Lin, Phys. Rev. D **106**, 064043 (2022)
41. J.T. Yao, X. Li, Phys. Rev. D **108**, 084067 (2023)
42. M. Rizwan, M. Jamil, A. Wang, Phys. Rev. D **98**, 024015 (2018)
43. B. Toshmatov, Z. Stuchlik, B. Ahmedov, Eur. Phys. J. Plus **132**(02), 98 (2017)
44. S. Fernando, Gen. Relativ. Gravit **45**, 2053 (2013)
45. S. Fernando, Int. J. Mod. Phys. D **22**(13), 1350080 (2013)
46. H. Nariai, Sci. Rep. Tohoku Univ. Ser. I **35**, 62 (1951)
47. V. Cardoso, A.S. Miranda, E. Berti, H. Witeck, V.T. Zanchin, Phys. Rev. D **79**, 064016 (2009)
48. R. Shaikh, P. Kocherlakota, R. Narayan, P.S. Joshi, Mon. Not. R. Astron. Soc. **482**(01), 52 (2019)
49. A. Abdujabbarov, M. Amir, B. Ahmedov, S.G. Ghosh, Phys. Rev. D **93**(10), 104004 (2016)
50. C. Bambi, Springer **10**, 978 (2017)
51. H. Shiyang, D. Chen, L. Dan, W. Xin, E. Liang, Eur. Phys. J. C **82**, 885 (2022)
52. V. Perlick, O.Y. Tsupko, Phys. Rep. **947**, 1 (2022)
53. Y. Mizuno, Z. Younsi, C.M. Fromm, O. Porth, M. De Laurentis, H. Olivares, H. Falcke, M. Kramer, L. Rezzolla, Nat. Astron. **2**, 585 (2018)
54. D. Psaltis, Gen. Relativ. Grav. **51**, 137 (2019)
55. A. Stepanian, S. Khlghatyan, V.G. Gurzadyan, Eur. Phys. J. Plus **136**, 127 (2021)
56. S. Vagnozzi, R. Roy, Y.D. Tsai et al., Class. Quantum Gravity **40**, 165007 (2023)
57. K. Akiyama et al., Astrophys. J. **875**, L2 (2019)
58. K. Akiyama, A. Alberdi, W. Alef, J.C. Algaba, R. Anantua, Astrophys. J. Lett. **930**, L12 (2022)